A New Boundary Layer Mixing Scheme. Part I: Scheme Description and Single-Column Model Tests

A. P. LOCK, A. R. BROWN, M. R. BUSH, G. M. MARTIN, AND R. N. B. SMITH

The Met. Office, Bracknell, United Kingdom

(Manuscript received 18 June 1999, in final form 14 February 2000)

ABSTRACT

A new boundary layer turbulent mixing scheme has been developed for use in the UKMO weather forecasting and climate prediction models. This includes a representation of nonlocal mixing (driven by both surface fluxes and cloud-top processes) in unstable layers, either coupled to or decoupled from the surface, and an explicit entrainment parameterization. The scheme is formulated in moist conserved variables so that it can treat both dry and cloudy layers. Details of the scheme and examples of its performance in single-column model tests are presented.

1. Introduction

Turbulence in the atmospheric boundary layer causes mixing of heat, moisture, and momentum that has to be represented in large-scale weather and climate prediction models that seek to describe the evolution of the mean profiles. Numerous studies (e.g., Beljaars and Betts 1992; Holtslag and Boville 1993) have demonstrated significant sensitivity of the results of such models to the boundary layer parameterization used.

One traditional approach has been to use a local first-order closure (e.g., Louis 1979) to represent the effects of boundary layer turbulence. This method relates the turbulent fluxes to the local mean gradients using an eddy diffusivity that itself is related to the local stability. In stable conditions, in which the turbulence is typically in local equilibrium, this approach appears to be well founded. However, there are a number of problems associated with the use of this method in unstable conditions. First of all, it takes no account of transports by large eddies that may span the boundary layer and lead to fluxes being much more dependent on overall layer stability than on local gradients. Typically, in order to sustain the required fluxes, a local closure will have to maintain excessive gradients across a boundary layer that in reality should be well mixed (e.g., Ayotte et al. 1996; Brown 1996). This may impact on the surface fluxes and can also lead to predictions of unrealistically large amounts of cloud at low levels (Holtslag and Boville 1993). Second, entrainment at the boundary layer top tends to be underestimated (e.g., Ayotte et al. 1996), often leading to modeled boundary layers that are too shallow, cold, and moist (Beljaars and Betts 1992). Finally, sensitivity to small changes in the local gradients means that such a scheme may not be very numerically robust (Beljaars 1991).

In response to the problems noted above, various new ''nonlocal'' schemes have been developed in recent years to represent mixing in unstable conditions. One such scheme is that proposed by Holtslag and Boville (1993, hereafter HB93), extending earlier work by Troen and Mahrt (1986). Rather than relating the diffusivities to local gradients, a profile shape is prescribed, and the magnitude is related to a turbulent velocity scale, which is determined from the surface forcing. Terms representing nonlocal fluxes of heat and moisture are also included. Entrainment effects are simply dealt with by choosing the definition of the boundary layer top such that the prescribed diffusivity profiles do not go to zero until some distance above the mixed layer tops. HB93 showed that implementation of this scheme (in place of a local one) led to much more realistic boundary layer structures in a global climate model. Nevertheless, it should be noted that the results do show considerable sensitivity to the definition of boundary layer top used. Different definitions may change the amount of entrainment, and some can undesirably lead to the boundary layer scheme mixing into cumulus layers (Vogelezang and Holtslag 1996). Furthermore, the scheme can only represent mixing in a single surface-based mixed layer and has no representation of turbulent processes driven from cloud top.

Van Meijgaard and van Ulden (1998) extended the HB93 scheme to allow for mixing driven by radiative cooling at the top of a stratocumulus cloud. A second

Corresponding author address: Dr. A. P. Lock, The Met. Office, Rm. 172, London Road, Bracknell, Berkshire RG12 2SZ, United Kingdom. E-mail: aplock@meto.gov.uk

diffusivity profile is specified within the cloud layer, with its magnitude proportional to a velocity scale related to the cloud-top radiative cooling. Entrainment effects are included by extending the diffusivity profile a distance above the cloud top that is related to the local stability. Van Meijgaard and van Ulden (1998) showed that this scheme performed well on a single quasi-stationary stratocumulus case study from the Atlantic Stratocumulus Transition Experiment (ASTEX), although some sensitivity to the details of the entrainment formulation was noted.

The present paper documents a scheme that extends this earlier work, as described in section 2, and is suitable for implementation in weather forecasting and climate prediction models. Single-column model results are presented in section 3 while tests in climate and forecasting models will be described in Martin et al. (2000, hereafter Part II).

2. Scheme description

In order to treat both dry and cloudy boundary layers in the same way, the scheme is formulated in the moist variables θ_l, the liquid–frozen water potential temperature, and q_t, the specific total water content. Because these variables are conserved under adiabatic vertical motion (in the absence of precipitation) eddy-diffusivity profiles can be used that span the whole depth of a well-mixed stratocumulus-capped boundary layer, in the same way as the large eddies that perform most of the transports do in reality.

The starting point and basis of the scheme is the identification of any unstable layers, be they clear or cloudy. This is done based on the buoyancy (allowing for latent heating effects) of undilute parcels lifted from the surface and lowered from the top of any layer cloud. When any unstable layers have been diagnosed, the next crucial step is to distinguish between those that are well mixed (i.e., clear and stratocumulus-capped layers), and those in which cumulus convection is present. This allows different mixing schemes to be applied in these two types of unstable layer. In well-mixed layers, fluxes are calculated using a nonlocal eddy-viscosity-based scheme based on that of HB93, but extended to allow for the effects of turbulence driven from cloud top, by radiative and evaporative cooling, as well as from the surface. Additionally, entrainment at the tops of well-mixed layers is parameterized directly using the scheme of Lock (1998). This avoids the problems, discussed in section 1, with sensitivity to how the eddy-diffusivity profiles might be extended into inversion. Cumulus layers are parameterized using a mass-flux convection scheme (Gregory and Rowntree 1990). Although this use of two discrete mixing schemes is to some extent undesirable, it has been found to be essential, as allowing the eddy-viscosity-based scheme to act in steady cumulus layers can rapidly result in them erroneously evolving into well-mixed stratocumulus, as discussed in Vogelezang and Holtslag (1996). Finally, a parcel descent is also used to calculate the depth of turbulent mixing driven from cloud top, thereby either allowing decoupling of stratocumulus-capped layers to be diagnosed or allowing the eddy-diffusivity profile representing turbulence driven from cloud top to span the full depth of the boundary layer [unlike the scheme proposed by van Meijgaard and van Ulden (1998)].

Inherent in this new scheme is the identification of layers of differing mixing regimes and their discrete treatment. This can best be illustrated by identifying six different types of boundary layer that are distinguished by the relative positions in the vertical of stable and unstable turbulently mixed layers and cumulus cloud layers. These are illustrated schematically in Fig. 1 and are discussed in more detail below, where details of the layer diagnosis, entrainment, and nonlocal mixing parameterizations are also given. Single-column model tests that demonstrate that the scheme is capable of switching reasonably smoothly and realistically between the different regimes in cases where such transitions are expected are presented in section 3.

a. Identification and classification of unstable layers

As noted above, the first step is to identify and classify any unstable layers so that the appropriate mixing parameterization can be applied. To identify convectively mixed layers driven from the surface (see types III–VI in Figs. 1c–f), a parcel is constructed from θ_l and q_t evaluated at 10 m, with the temperature increased by an amount equal to a term proportional to the surface kinematic buoyancy flux over a stability-dependent near-surface turbulent scaling velocity (as in HB93) plus 0.4 K. The constant is added purely to reduce the chances of any noise in the temperature profile leading to an erroneously small layer depth diagnosis (although, as described below, special steps are taken to ensure that real but weak decoupling inversions can be identified). The parcel is then lifted upward, allowing for any latent heating effects, and the top of the surface-based mixed layer (z_{sml}) is taken to be the height (z_{par}) at which this parcel is neutrally buoyant relative to the environment if below the lifting condensation level (LCL), or the height at which it has maximum buoyancy excess over the environment if above the LCL. Use of the height of maximum excess (rather than that of zero excess) is typically of little consequence in stratocumulus regions, but can be necessary in order to identify the capping inversion in cumulus cases (e.g., in the trade wind regions).

Any surface-driven unstable layers thus identified are categorized as ''well mixed'' (types III or IV, the latter being identified later as decoupled) or ''cumulus capped'' (types V or VI, the former being capped by a decoupled stratocumulus layer; see below) based on the gradients of the mean profiles [a discussion of typical boundary layer profiles can be found in Betts (1986), e.g.]. Specifically, the presence of cumulus is diagnosed if the

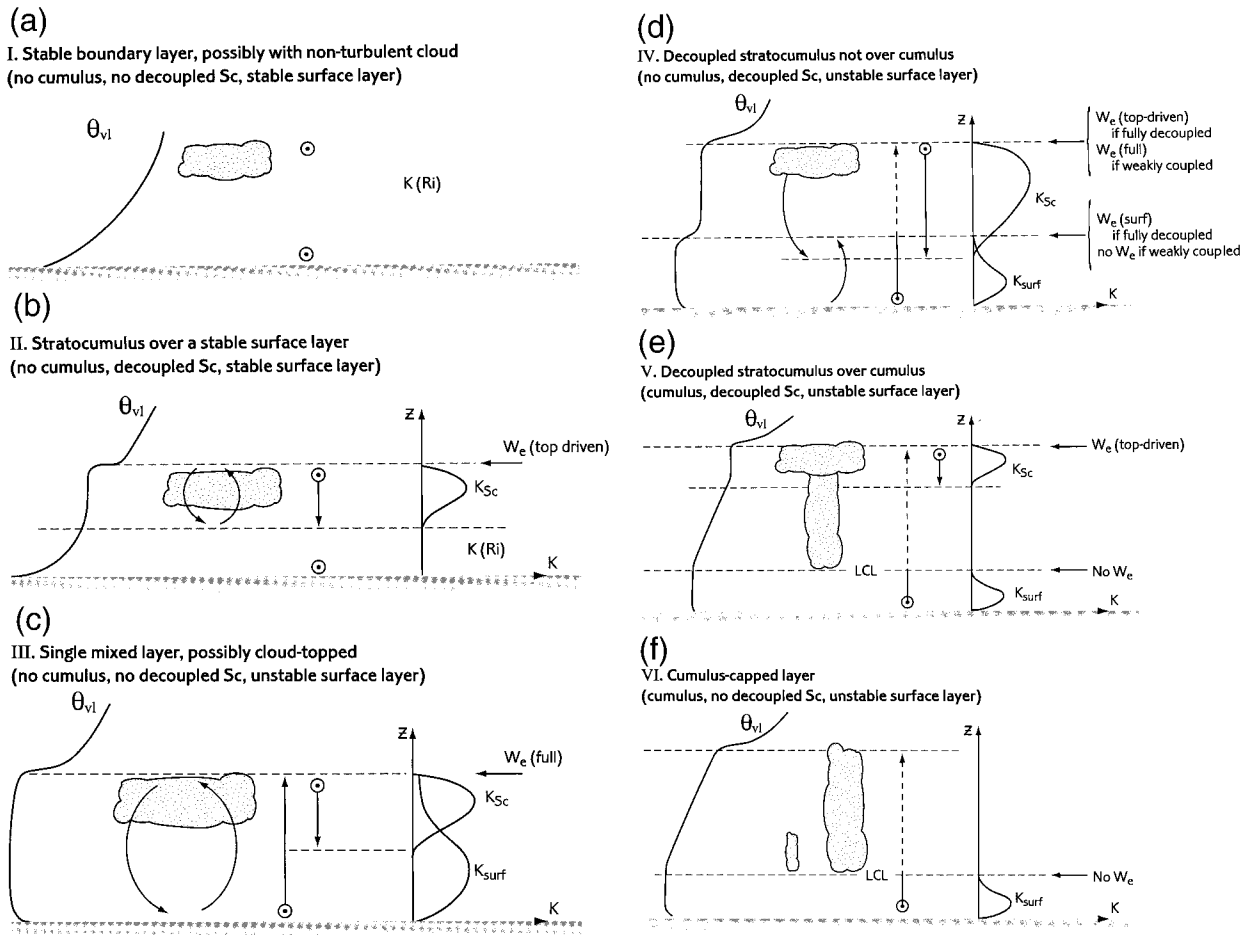

FIG. 1. Schematic representation of the six boundary layer types. The tops of the upward arrows indicate the height of z_{par} while the tops of their respective solid lines indicate z_{sml}.

magnitude of the mean gradient of q_t between the LCL and z_{par} is greater than a threshold factor times the magnitude of the mean gradient below the LCL. Currently the threshold factor is set to 1.1. In this case, the top of the surface-based mixed layer (z_{sml}) is set to the height of the LCL (rather than to z_{par}, as illustrated in Figs. 1e,f for types V and VI) so that mixing through the cumulus cloud layer is only carried out by the model's mass-flux convection scheme and not by the eddy-viscosity-based boundary layer scheme. Note that, for type V in Fig. 1e, the mass-flux scheme operates up through decoupled stratocumulus layers in which the eddy-viscosity-based scheme is also operating (representing the more homogeneous mixing driven from the stratocumulus cloud top), much as is observed in reality [e.g., during the ASTEX observational campaign (Martin et al. 1995)].

The presence and depth of any layer unstable to mixing driven by buoyancy sources at cloud top (types II–V in Figs. 1b–e) is diagnosed by moving a second parcel downward from the top of any cloud layer at or above z_{par} that has a layer cloud fractional area [as diagnosed independently by the model's cloud scheme (Smith 1990)] greater than a threshold value (currently 0.1). This diagnosis is restricted to approximately the lowest 2.5 km of the model domain as only these levels (currently 14) are processed by the boundary layer scheme. Note that there is no requirement within the scheme for cloud-top-driven convection to extend to the surface and therefore decoupled cloud layers can be modeled. Note also that this diagnosis is independent of the surface stability and so decoupled stratocumulus over a stable surface can be modeled (type II in Fig. 1b).

In reality, the buoyancy of downdrafts in cloud-capped layers will depend primarily on the balance between cloud-top radiative cooling, entrainment warming, and evaporative cooling. This presents two obstacles to determining whether a cloud layer is convectively unstable. First, the true buoyancy of the parcel will be strongly dependent on the evolution of its liquid water content and the degree of evaporative cooling it experiences, which is in turn strongly dependent on the evolution of its mixing fraction of cloudy and entrained air during its descent through the cloud. Such a parcel model would be too complex in a parameterization of

this sort and would introduce many additional uncertainties. However, Lock (1998) discussed how top-driven mixing might predominantly be expected to extend to below cloud base, in the absence of any existing decoupling inversion. Thus, it should be sufficient to use the moist conserved variable θ_{vl} [$=\theta_l(1 + 0.608q_t)$, which is equal to the virtual potential temperature in cloud-free air] in order to have an accurate measure of the buoyancy of parcels descending adiabatically from cloud top once they are below cloud base. The second obstacle is that the amount of entrainment is still to be determined since it depends on the layer depth. Thus, a preliminary parcel descent is made by perturbing the cloud-top θ_{vl} by an amount equal to the cloud-top radiative cooling rate, multiplied by an assumed cloud-top residence timescale for mixed-layer eddies (currently set to 500 s). The grid level at which this parcel's θ_{vl} exceeds that of the environment is used to estimate the depth (z_{d1}) of the decoupled mixed layer in the entrainment rate parameterization (which has only a weak dependence on the layer depth, z_{ml}, as described in the appendix). Note that the layer will only be diagnosed as unstable if the parcel descends more than one level.

Once the entrainment rates for any unstable layers have been calculated (as described in section 2b), the depths over which the top-driven eddy-diffusivity profiles are to be specified must be evaluated. As these depths could be important to the subsequent evolution of the cloud layers, additional parcel descents are made using the entrainment rates just calculated. This time the top of the layer θ_{vl} (θ_{vl}^{top}) is perturbed by the combined effects of the radiative and entrainment fluxes on the parcel, scaled by the parameterized velocity scale representative of the top-driven turbulence ($V_{Sc}^3 = V_{rad}^3 + V_{br}^3$, as defined in the appendix). For the parcel, then,

$$\theta_{vl}^{par} = \theta_{vl}^{top} + \frac{w_e \Delta\theta_{vl} - \Delta_F}{V_{Sc}},$$

where w_e is the entrainment rate, $\Delta\theta_{vl}$ is the grid-level change in θ_{vl} across the inversion, and Δ_F is the net radiative divergence across the top cloudy grid level. As before, the parcel descent is stopped once it has an excess θ_{vl} over the environment to give an estimate for the depth of the mixing, z_{d2}. As discussed above, however, because θ_{vl} rather than buoyancy has been used for the parcel descent, a further assumption is made that top-down mixing will extend to at least 1.2 times the cloud depth (z_c) below the inversion unless the original radiatively determined parcel descent stopped within the cloud layer (assumed to indicate the presence of an inversion within the cloud layer). The use of a factor greater than unity is an empirical result taken from the large eddy simulations (LES) presented in Lock (1998). Thus, the vertical extent of the top-driven eddy-diffusivity profiles (z_d) is taken to be

$$z_d = \max[z_{d2}, \min(1.2z_c, z_{d1})].$$

Typical parcel ascents and descents and profiles of θ_{vl} are shown for the six boundary layer types in Fig. 1. This also illustrates, for type IV, a further aspect of this part of the scheme that aims to identify stratocumulus layers that are decoupled from the surface only by inversions of $\lesssim$0.5K, such as were observed in daytime during the First International Satellite Cloud Climatology Program (ISCCP) Regional Experiment (FIRE), for example (see Hignett 1991). It is quite possible that the temperature perturbation applied to the surface-based parcel could be sufficient for the ascent to miss such an inversion and the magnitude of the resulting eddy diffusivity profile could be large enough to remove it. Consequently, if a well-mixed cloud-capped boundary layer is diagnosed, a further test on the local gradients within the layer is carried out and if a positive maximum of the local θ_{vl} gradient greater than 10^{-3} K m^{-1} is found, z_{sml} is set to the height of this inversion. Note that the purpose (and immediate effect) of this test is to restrict the height to which surface-driven mixing can be applied and so allow decoupling to proceed—if the various processes in the separate layers are acting to increase the buoyancy of the upper layer relative to the lower then this restriction should allow an inversion to form between them. If this diagnosis of a decoupled layer were erroneous (due to noise in the profile, e.g.), it is anticipated that the processes in the separate layers would then be acting to reduce the buoyancy difference between them making subsequent misdiagnosis less likely. In the meantime, top-down mixing might be expected to sustain mixing down to the surface. These arguments are also taken into account when the positioning of the specified entrainment is determined, as discussed in section 2b.

Note that much of the above detail is necessary only to ensure that the scheme can be implemented safely in a global model. It represents an initial attempt at least to *allow* decoupling of stratocumulus layers, an important process currently not well understood. Although the scheme appears to give a reasonable climatology of well-mixed and decoupled stratocmulus layers (as described in Part II), the decoupling diagnosis has been found to be somewhat time step and resolution dependent in single-column model tests (as discussed in section 3). Consequently, alternative strategies, such as that proposed by Turton and Nicholls (1987) based on integrals of the buoyancy flux profile, are currently being tested and preliminary results suggest such an approach may be more robust.

Finally, the inversion identified by these methods can also be lowered a grid level if the θ_{vl} gradient between the two levels below is greater than 10^{-3} K m^{-1}, as this indicates the inversion is spread over two levels and it is important that the entrainment parameterization be applied at its base.

b. Entrainment parameterization

From numerous LESs, Lock (1998) identified and parameterized three velocity scales representative of the

buoyancy sources of turbulence. These were $V_{\rm surf}$, $V_{\rm rad}$, and $V_{\rm br}$, representative of surface heating, cloud-top radiative cooling, and buoyancy reversal (by evaporative cooling of entrained air), respectively. Their definitions are given in the appendix. Additionally, following Driedonks (1982), the effects of shear production of turbulence on the entrainment rate have been simply related to the surface friction velocity, u_*. The parameterization of the entrainment rate, w_e (given, in the absence of subsidence, by the rate of rise of the inversion), used in the model can be written (using the notation given in the appendix)

$$w_e = A_1 \frac{V_{\rm sum}^3/z_{\rm ml} + g\tilde{\beta}_T \alpha_t \Delta_F}{\Delta b + c_T V_{\rm sum}^2/z_{\rm ml}}, \qquad (1)$$

where $V_{\rm sum}^3 = V_{\rm surf}^3 + V_{\rm rad}^3 + V_{\rm br}^3 + A_2 u_*^3$. The constant A_1 is given a value 0.23, as in Lock (1998), and A_2 is set to 25, as in Driedonks (1982). To allow for weak inversions, the Zilitinkevich (1975) correction is included in (1) with the constant, $c_T = 1$. Lock (1998) also proposed a parameterization for α_t, which is the fraction of the cloud-top radiative divergence (Δ_F, in K m s^{-1}) that occurs across the horizontally averaged inversion in the LES, but in the current implementation this has only been given the constant value 0.2. Note that Lock postulated that this term arose from mixed-layer-scale undulations in the cloud top causing part of the cloud-top radiative cooling to occur within the horizontally averaged inversion, a conclusion also reached by Moeng et al. (1999). This cooling was found to promote deepening of the layer directly (as well as through generation of mixed-layer turbulence) and so should be included in (1) as these undulations will not be resolved in the model.

This parameterization is implemented within the first-order turbulence closure by specifying the fluxes of the conserved variables, θ_l and q_t, at the grid level spanning the inversion (at $z = z_i$, say). This can be achieved, as discussed in more detail in the appendix of Lock (1998), by specifying the eddy diffusivity for scalar variables, K_h, for example, at this level as

$$K_h|_{z_{\rm fl}} = w_e \Delta z|_{z_{\rm fl}}, \qquad (2)$$

where $\Delta z|_{z_{\rm fl}}$ is the model grid spacing at the inversion. The entrainment eddy diffusivity for momentum, K_m, is set equal to $K_h|_{z_{\rm fl}}$ multiplied by a turbulent Prandtl number of 0.75. As a result of (2), the entrainment flux of q_t, for example, is specified as

$$\overline{w'q_t'}|_{z_{\rm fl}} = -K_h|_{z_{\rm fl}} \left.\frac{\Delta q_t}{\Delta z}\right|_{z_{\rm fl}} = -w_e \Delta q_t|_{z_{\rm fl}}. \qquad (3)$$

Thus, assuming a discontinuous inversion, the flux specified at the model's inversion by this method should allow the mixed layer to deepen at the rate given by w_e or maintain the correct balance in the presence of subsidence.

Further aspects of the implementation of the entrainment parameterization are illustrated in Fig. 1. Given the form of (1), the parameterization can readily be split into contributions from surface-based processes, w_e(surf), and cloud-top processes, w_e(top driven). When there is no cumulus convection diagnosed, the height at which w_e(surf) is applied is chosen to depend on the degree of decoupling between the surface and the elevated turbulent cloud layer. As discussed in section 2a, a diagnosis of decoupling in well-mixed cloud layers is made (based on the $\theta_{\rm vl}$ gradient within the layer) in order to restrict the extent of surface-driven mixing and thus allow decoupling to proceed if conditions are favorable. It was argued that any erroneous diagnosis might be expected to have few negative repercussions and these are alleviated further by introducing a ''weakly coupled'' state for otherwise decoupled layers (see type IV in Fig. 1d). This is determined by the $\theta_{\rm vl}$ difference between the two layers being less than 0.2 K and results in the full w_e being applied at cloud top. If this is not the case, then w_e(surf) is applied at $z_{\rm sml}$ and only w_e(top driven) at cloud top. Note that the term involving u_*^3 contributes to w_e(surf), which means that, at present, there is no representation of enhanced entrainment rates due to shear across the top of a decoupled stratocumulus layer. In addition, no surface-driven entrainment parameterization is applied anywhere if cumulus is diagnosed, as the required transports through the LCL are performed by the model's convection scheme.

c. Flux parameterization in well-mixed layers

As described in the introduction, profiles of eddy diffusivity are specified over the depths of the mixed layers, as diagnosed above. For turbulence driven from the surface, the profiles are similar to those in HB93, except that here the profile is adjusted so that it tends to the specified entrainment eddy diffusivity, $K_h|_{z_{\rm fl}}$ [given by (2)] at the inversion. Using $K_h^{\rm surf}$ for convective conditions as an example,

$$K_h^{\rm surf} = 0.85\kappa V_{\rm surf} z \left(1 - \mathcal{E}\frac{z}{z_i}\right)^2. \qquad (4)$$

Setting $K_h^{\rm surf} = K_h|_{z_{\rm fl}}$ at $z = z_i$, (4) can be rearranged to give $\mathcal{E}$ (although in order to avoid altering the shape function too much, the value of $\mathcal{E}$ used is not allowed to fall below 0.7). Otherwise, for the surface-driven mixing profiles, the formulation of the velocity scale and the variation of the Prandtl number (given by K_m/K_h, where K_m is the eddy diffusivity for momentum) follow HB93.

As described in Lock (1999), profiles of K_m and K_h for top-driven mixing are specified over mixed layers (between $z = z_b$ and z_i, say), which are similar to upside-down versions of (4) except that, as suggested by LES, the shape function is larger close to the turbulence driving interface. The top-driven K_h, for example, is given by

$$K_h^{\rm Sc} = 0.85kV_{\rm Sc}\frac{z'^2}{z_{\rm ml}}\left(1 - \frac{z'}{z_{\rm ml}}\right)^{0.5}, \qquad (5)$$

where $V_{Sc}^3 = V_{rad}^3 + V_{br}^3$ and $z' = z - z_b$. A fixed Prandtl number of 0.75 is used to obtain K_m^{Sc}.

Typical profiles are shown as K_{surf} and K_{Sc} in Fig. 1. The profiles may overlap, or they may not, indicating in the latter case the presence of a turbulent cloud layer that is decoupled from the surface. Mixing coefficients K(Ri) based on the the local Richardson number (as in Smith 1990) are also calculated. They are used in stable layers, and also in unstable layers, if they are larger than the nonlocal coefficients. The vertical flux of a quantity, χ, is given by

$$\overline{w'\chi'} = -\max[(K_\chi^{surf} + K_\chi^{Sc}), K_\chi(\mathrm{Ri})]\frac{\partial\overline{\chi}}{\partial z} + K_\chi^{surf}\gamma_\chi, \quad (6)$$

where K_χ is the appropriate diffusivity (K_m for momentum, K_h for scalars). The last term on the right-hand side represents a nonlocal flux. Currently it is only related to surface forcing and is nonzero only for $\chi = \theta_l$, in which case the countergradient term, γ_{θ_l}, is calculated as in Holtslag and Boville (1993). The effect of including this term is to allow the model to maintain more well-mixed θ_l profiles. The surface-based nonlocal flux for q_t is set to zero in order to represent crudely the effects on the mixed-layer q_t profile of entrainment drying at the mixed-layer top, which tend to make q_t profiles less well mixed than those of θ_l (Mahrt 1976). It is planned to introduce a more complete nonlocal flux parameterization, which allows for both surface and entrainment fluxes in a consistent manner, such as that described in Cuijpers and Holtslag (1998).

In all, six different types of boundary layer can be represented by this scheme, as shown schematically in Fig. 1. The new scheme has been tested in single-column, climate, and numerical weather prediction versions of the U.K. Met. Office (UKMO) Unified Model. Results will be presented here from the single-column model and, in particular, the ability of the scheme to switch realistically between the different boundary layer types will be emphasized.

3. Single-column model tests

The single-column model (SCM) used is a one-dimensional (vertical) configuration of the UKMO Unified Model. In addition to the boundary layer parameterization described here, cumulus convection is parameterized using the mass-flux scheme of Gregory and Rowntree (1990). Layer cloud liquid water and cloud fraction are diagnosed following Smith (1990) and precipitation from layer cloud is as in Senior and Mitchell (1993), a bulk scheme with parameterized autoconversion and accretion. Radiative fluxes are calculated using a general two-stream radiation scheme (Edwards and Slingo 1996). In order to represent direct interactions between, for example, cloud-top radiative cooling and turbulence generation accurately, the new boundary layer mixing scheme is explicitly dependent on quantities, such as the net radiative divergence and cloud fraction, which are currently calculated independently in the model. While the results will quite rightly be dependent on the output from these other schemes, there should be no difficulty in principle in implementing the scheme in another model with different parameterizations of these processes.

A number of SCM simulations have been performed to test this scheme. The three presented here were driven by prescribed large-scale divergence, geostrophic winds, and, for the first two, sea surface temperatures (SST; with the surface fluxes calculated using Monin–Obukhov similarity theory), and prescribed surface fluxes for the third. The geostrophic wind is held constant at $(-10, -3)$ m s^{-1} in the first two simulations and $(10, 0)$ m s^{-1} in the third. A 10-min time step is used and there are 14 pressure levels below approximately 750 hPa (for a surface pressure of 1020 hPa) with the spacing stretched away from the surface. This is the resolution used when the scheme is implemented in the global models and gives around 200-m resolution between 500 and 1500 m, for example.

In addition to the scheme as described in section 2, the increments from the mass-flux scheme used to parameterize cumulus convection were mixed uniformly over the surface-based mixed layer. This was because the model's time step is formulated in such a way that the mass-flux scheme is called after the boundary layer scheme has updated the model fields. Mixing these increments should therefore allow the model to better maintain a well-mixed layer. In principal, the mass-flux increments should be similarly mixed over decoupled layers but that has not yet been implemented. Also, the mass-flux scheme was stopped from operating within the boundary layer (including any decoupled cloud layers) unless the boundary layer scheme diagnosis indicated the presence of cumulus convection. Without this constraint, the mass-flux scheme could approximately reproduce the mixing performed by the boundary layer scheme, leading to the double-counting of entrainment, for example. These changes, which are still to be tested in the large-scale models described in Part II of this paper, represent initial attempts to couple the boundary layer and mass-flux mixing schemes. It is intended to extend them to include, for example, explicit triggering of the mass-flux scheme based on the boundary layer scheme diagnosis.

a. Equilibrium stratocumulus

The first simulation has constant surface and large-scale forcing, with SST = 291.4 K and a large-scale divergence of 2.5×10^{-6} s^{-1}. The initial profiles are based on measurements made by the Meteorological Research Flight C-130 Hercules aircraft during FIRE (see Albrecht et al. 1988): the boundary layer has uniform values of $\theta_l = 290$ K and $q_t = 8$ g kg^{-1}, which gives a cloud layer some 500 m thick, with cloud top at around 1100 m. The jumps across the inversion are approximately 14 K and 6 g kg^{-1}. Incoming solar radiation and Coriolis parameter appropriate to 30°N are

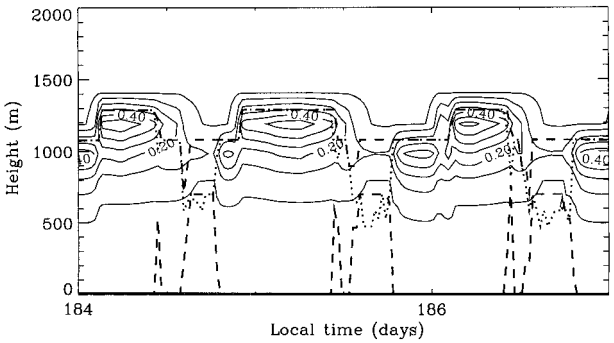

FIG. 2. A time–height contour plot of q_l from an SCM simulation of stratocumulus. The dotted line is the height of the top of the surface-driven turbulent layer (z_{sml}) and the dashed lines indicate the highest extent of turbulent mixing (z_{top}) and the lower boundary of any well-mixed decoupled cloud layer.

used. The purpose of this simulation is to examine the diurnal variation of a stratocumulus sheet otherwise approximately in equilibrium with its forcing, such as is often observed in subtropical stratocumulus, rather than to match a particular observation.

Figure 2 shows a contour plot of three days of the time evolution of the layer cloud liquid water mixing ratio, q_l, together with the mixed-layer boundaries. Shown are the highest extent of any turbulent mixing (z_{top}, dashed line), the top of the surface-based mixed layer (z_{sml}, dotted line), and the base of any decoupled layer (dashed line). The time axis is local time in Julian days. It is apparent from Fig. 2 that the model is qualitatively representing the observed features of subtropical stratocumulus very well (see Hignett 1991, e.g.). During the night the cloud thickens and cloud top starts to rise (as strong radiative cooling of the cloud top cools the layer and drives relatively strong entrainment). After sunrise (at around 0500 local time) the generation of entrainment weakens and so cloud top drops. At or around local noon, when shortwave heating is at its strongest, the otherwise predominantly top-driven turbulent mixing is made relatively weak and stable gradients form within the layer, leading to the decoupling evident in Fig. 2. Shortly before sunset, strong cloud-top cooling leads to a recoupling of the cloud layer with the surface, and the cloud thickens and starts to rise again. More quantitatively, the liquid water path varies diurnally between 180 and 20 g m^{-2}, which again is typical of observations.

b. Stratocumulus to trade cumulus transition

The second simulation illustrates the transition from well-mixed stratocumulus (Sc) to trade cumulus (Cu) that occurs in the subtropics as air moves over a progressively warmer sea surface and subsidence weakens. The simulation is based on that described in Bretherton et al. (1999), which was driven by the SST and large-scale divergence observed in the first ASTEX Lagrangian experiment, which took place near the Azores (see de Roode and Duynkerke 1997). Figure 3 shows the time evolution of q_l, the boundary layer type, and the mixed-layer boundaries. The results compare well against the observations and, more importantly, they show relatively smooth transitions between boundary layer types. Initially the surface layer is stable (with turbulent mixing calculated using the local Ri-based scheme) and the overlying stratocumulus, in which nonlocal top-driven mixing is operating, is decoupled from it (type II). Once the sun sets, cloud-top radiative cooling, and the increased turbulent mixing associated with it, causes the base of the decoupled layer to fall until, with the surface sensible heat flux becoming positive at around day 170.1, the layer becomes well mixed to the surface (type III) and the nonlocal scheme takes over completely. Shortly after sunrise (at about day 170.2), decoupling is diagnosed (type IV) and, shortly after noon, cumulus is diagnosed (type V) and the mass-flux convection scheme is triggered (despite the current lack of an explicit link between the two schemes); cumulus was observed under the stratocumulus at this time during flight 3. After sunset (at about day 170.8) the scheme briefly, and perhaps somewhat erratically, predicts top-driven mixing almost down to the surface. Unfortunately, no observations were made at this time but it is not impossible that strong cloud-top radiative cooling could briefly have led to recoupling. However, a coupled layer cannot be sustained for long as the stratocumulus rises rapidly to produce a well-mixed decoupled cloud layer overlying cumulus.

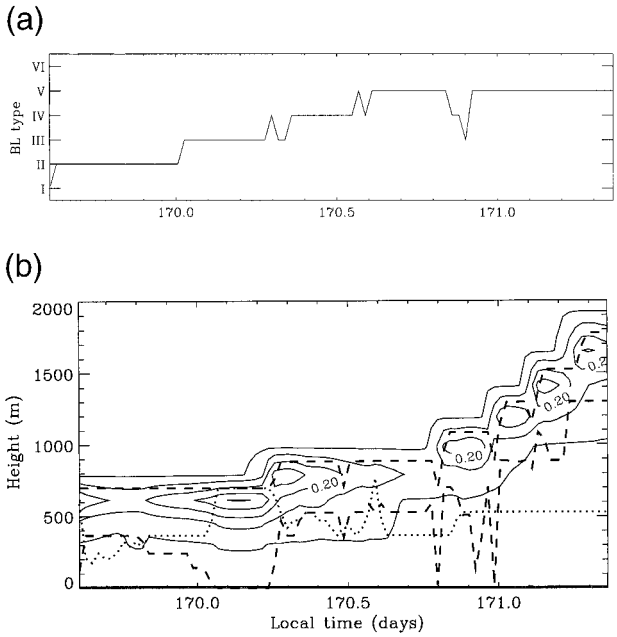

FIG. 3. The time series of boundary layer type and the time–height contour plot of q_l, as in Fig. 2, but from an SCM simulation of the first ASTEX Lagrangian experiment.

Figures 4 and 5 show profiles of the thermodynamic variables, the parameterized eddy diffusivities (K_h^{surf} and K_h^{Sc}), and the resulting turbulent flux of q_t at days 170.1

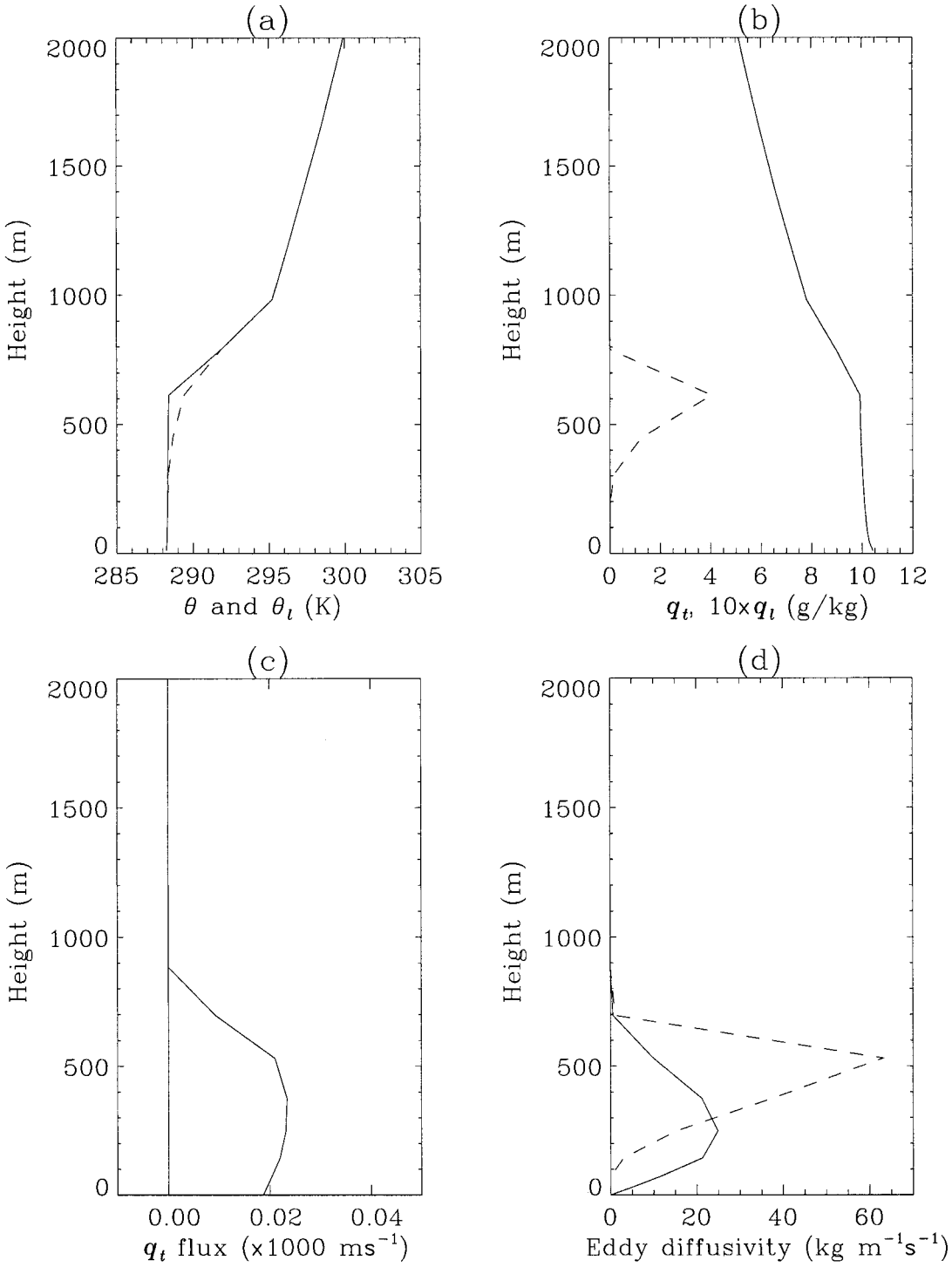

FIG. 4. Profiles of (a) θ_l (continuous line) and θ (dashed line), (b) q_t (continuous line) and q_l (dashed line), (c) $\overline{w'q_t'}$, and (d) K_h^{surf} (continuous line) and K_h^{sc} (dashed), averaged over the half hour previous to day 170.1 from the SCM simulation of the first ASTEX Lagrangian experiment.

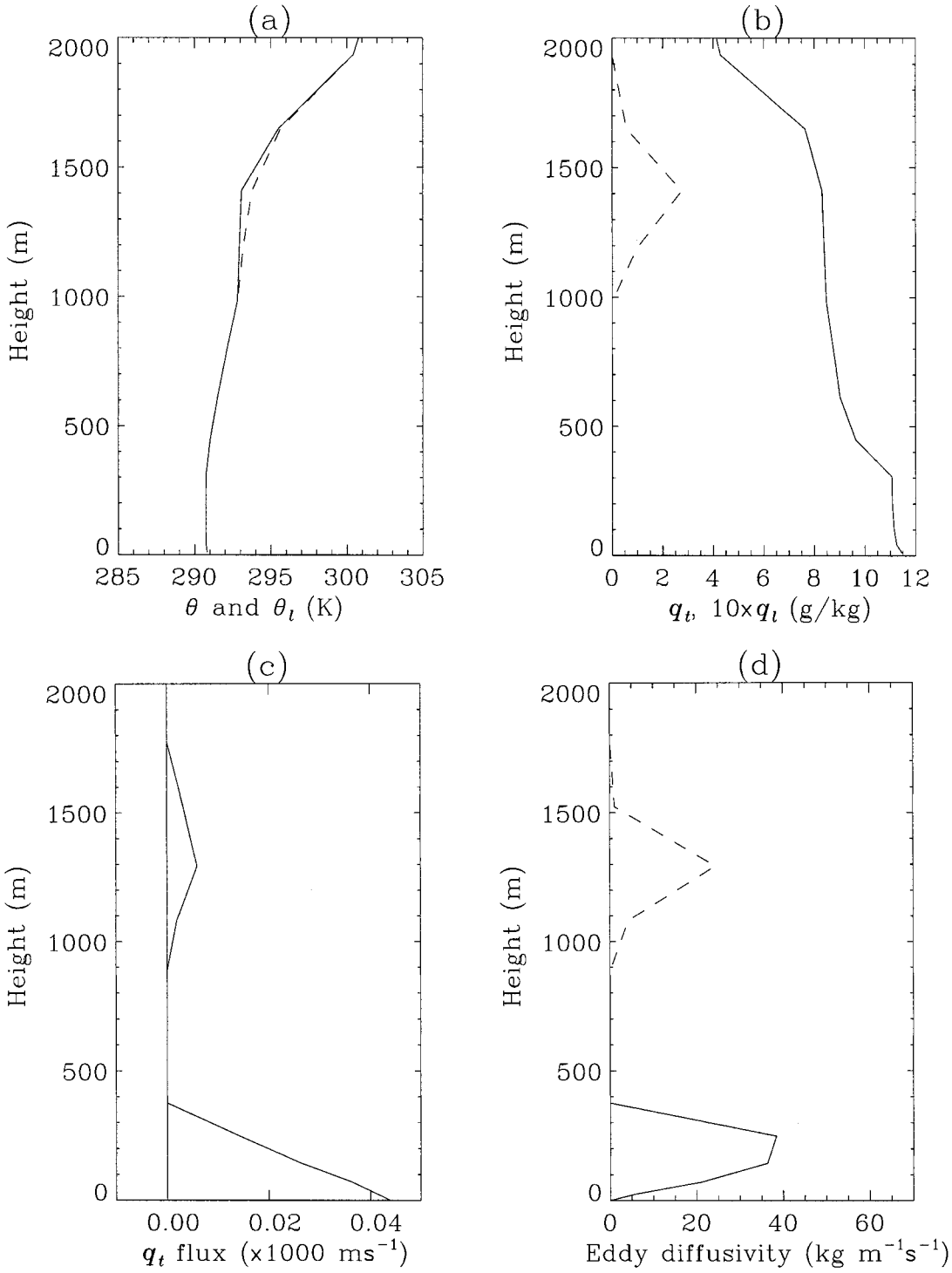

FIG. 5. As Fig. 4 but for day 171.2 of the ASTEX Lagrangian experiment.

and 171.2, respectively. The former time is during the well-mixed phase of the simulation, when both K_h^{surf} and K_h^{Sc} span the entire layer (Fig. 4d); note that the lack of linearity in $\overline{w'q_t'}$ in Fig. 4c at this time is because this model diagnostic does not include the drizzle flux. The latter time is when there is decoupled stratocumulus overlying cumulus; note the turbulent flux and K_h^{Sc} associated with top-driven mixing in the decoupled layer evident in Figs. 5c and 5d. Note also that the entrainment eddy diffusivities tend to be very small relative to the

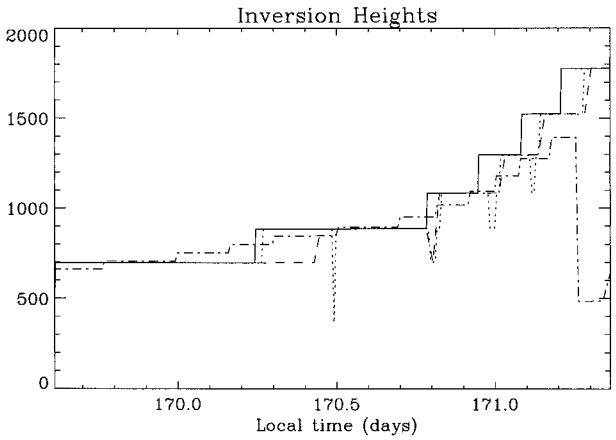

FIG. 6. The time series of boundary layer height, z_{top}, from SCM simulations of the first ASTEX Lagrangian experiment: standard resolution with 5-, 10-, and 30-min time steps (continuous, dotted, and dashed lines, respectively) and high resolution (dash–dotted line).

mixed-layer values because of the much larger gradients in the mean variables across the inversion. For a typical $w_e \sim 5 \times 10^{-3}$ m s^{-1}, (2) implies $K_h|_{z_{fl}} \sim 1$ m^2 s^{-1}.

The numerical robustness of the new scheme can be seen in Fig. 6, which shows the evolution of z_{top} for this case from the standard simulation (10-min time step, approximately 200-m resolution) together with three further simulations. Two have the standard resolution with 5- and 30-min time steps while the third has much finer resolution (at approximately 50 m) with a 10-min time step. There is very little sensitivity, then, in this important parameter, particularly during the first day. In the second half of the simulation, where decoupled stratocumulus begins to overlie cumulus convection, the diagnosis of the depth of decoupled layers is found to be more sensitive to time step and resolution, tending to give a more prolonged well-mixed diagnosis around day 171 than was seen in Fig. 3, although always decoupling by day 171.2. This sensitivity is perhaps to be expected given the nature of this aspect of the scheme and it has, in part, motivated our testing of alternative strategies (as discussed in section 2a).

This simulation was chosen as a stringent test of the scheme's ability to move from one mixing regime to another. It passes through all of types II–V referred to in Fig. 1, apparently realistically and relatively smoothly.

c. The formation of shallow cumulus over land

Finally, the scheme was tested on a case of daytime formation of shallow cumulus over land. The simulation is based on data from the Southern Great Plains Atmospheric Radiation Measurement program (ARM) site (R. Cederwall 1999, personal communication) and has prescribed surface fluxes for a diurnal cycle, a fixed geostrophic wind of 10 m s^{-1}, and no large-scale forcing or radiative fluxes. An LES has also been performed, with the same forcing and initial profiles, to give some indication of how well the SCM is performing. The LES model is that used in Brown (1999). This case demonstrates the ability of the scheme to switch first from stable to unstable surface forcing and, second, from a cloud-free well-mixed layer to a cumulus-capped layer. As with the ASTEX Lagrangian simulation, this latter transition tests the diagnosis of cumulus in the scheme, without which a gradually deepening well-mixed layer would be formed.

Figure 7 shows profiles at 3-h intervals from both the LES and SCM. The simulations start at around dawn (0530 local time) with a relatively shallow nocturnal stable boundary layer. The surface buoyancy flux increases rapidly, becoming positive within the first hour, and for the subsequent 3 h a well-mixed cloud-free boundary layer is formed (and diagnosed by the boundary layer scheme); note the buoyancy flux profile (dotted line in Fig. 8) produced by the SCM, with a negative entrainment flux around the inversion, which is typical of this regime. Around 0930 local time, the boundary layer scheme diagnoses a cumulus-capped boundary layer and continues to do so until the surface flux becomes negative again at around 1700. The boundary layer fluxes (including the entrainment flux) are therefore set to zero from the LCL upward (which rises during the day), as can be seen in Fig. 8. Although there is currently no explicit triggering of the mass-flux scheme from the boundary layer diagnosis, cumulus convection is initiated in the model, as can be seen from the adjustment of the profiles in Figs. 7c and 7d above where the boundary layer scheme has been switched off. Cumulus clouds were also first seen in the LES at around 0930. In both the LES and SCM cumulus convection continues through the day, with the cloud layer deepening, until the surface buoyancy flux becomes negative again. Note that the good agreement seen in Fig. 7 could not be achieved without adjusting the standard lateral entrainment and detrainment rates used in the mass-flux scheme (as described in Gregory and Rowntree 1990), as suggested both by the LES performed of this case and previous LES of marine shallow cumulus (see, e.g., Siebesma and Cuijpers 1995): the standard lateral entrainment rate was multiplied by a factor of 3 (to make it comparable with that seen in this LES) and the lateral detrainment rate was set to 1.5 times the lateral entrainment rate.

No problems, then, are apparent with the new boundary layer scheme's diagnosis of cumulus convection. An area of current work, however, is how better to match the transports performed by the two schemes across the lifting condensation level. It is discrepancies in this transport that are responsible for the ''stepping'' seen around the LCL, particularly in the q_t profiles (see Fig. 7d), when both are operating.

4. Conclusions

A new scheme for parameterizing turbulent mixing in large-scale models has been developed. It combines

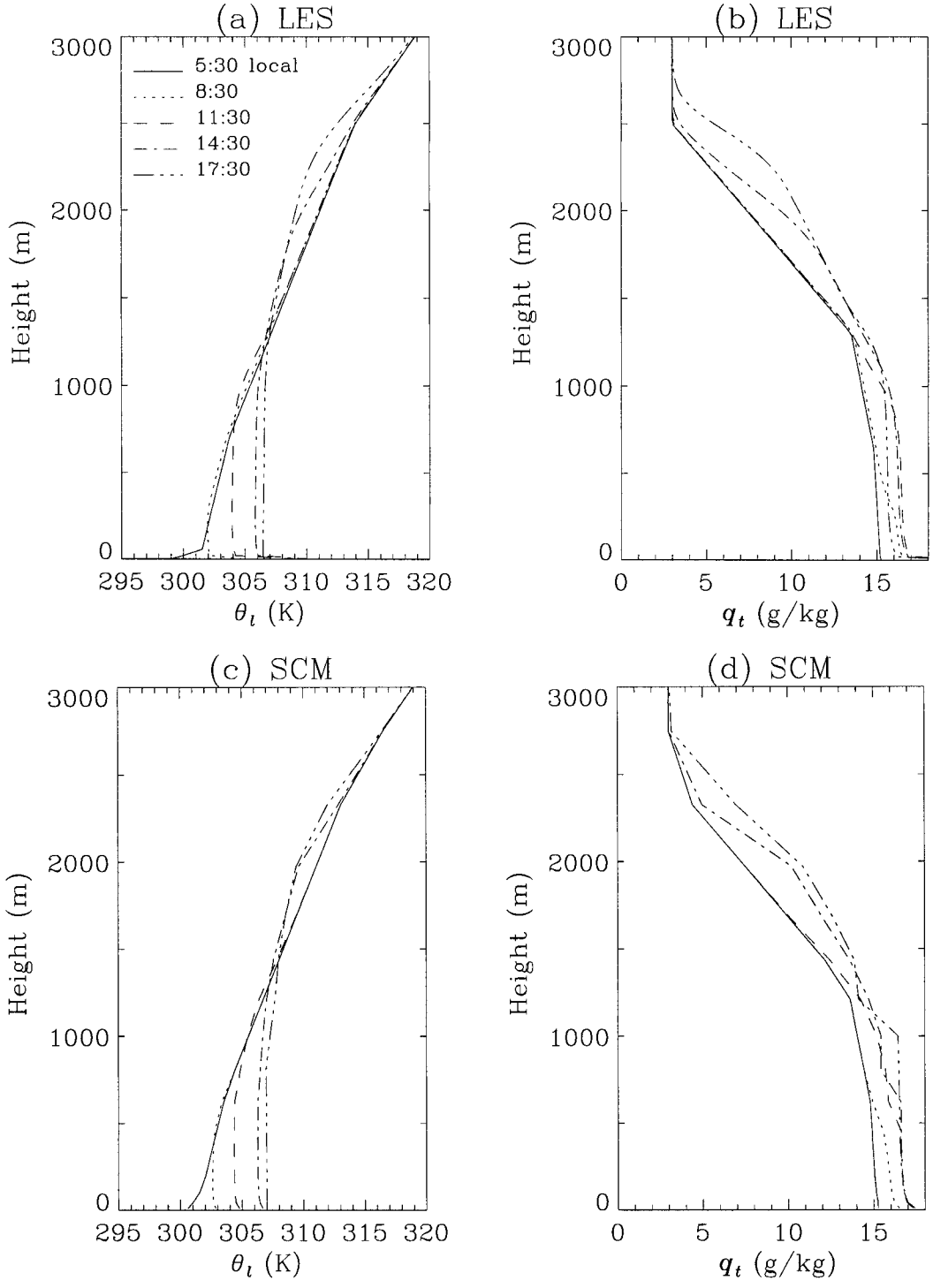

FIG. 7. Profiles of θ_l and q_t from the simulation of cumulus formation over land. (a) and (b) From the LES, with profiles averaged over the hour spanning the local times shown in the legend in (a), and (c) and (d) from the SCM, averaged over the half hour previous to those times.

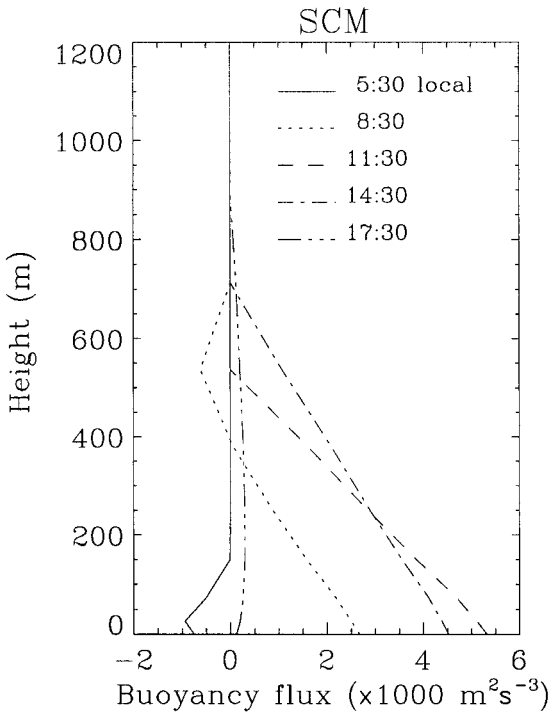

FIG. 8. Profiles of buoyancy flux, averaged over the half hour previous to the times shown in the legend, from the SCM simulation of cumulus formation over land.

nonlocally determined eddy-diffusivity profiles, for turbulence driven from both the surface and cloud top, with an explicit parameterization for the entrainment rate. It does this in a physically rational manner through the use of moist conserved thermodynamic variables that allow the profiles to span both the cloud and subcloud layers. The eddy diffusivities are scaled on the turbulence sources using results derived from large eddy simulations, thereby directly relating the turbulence intensity to the forcing mechanisms. This should make the scheme more robust in its operation than, for example, local first-order closures, which have been found sensitive to small changes in the local gradients. It attempts to distinguish between the mixing regimes associated with different boundary layer types and specify mixing parameterizations accordingly. This involves the diagnosis of cumulus-capped layers and of the decoupling of stratocumulus-capped layers. The latter is an essential process for which explicit parameterization is hampered by a current lack of understanding.

Single-column model studies presented here suggest that such an approach can be applied successfully and Part II of this paper describes the impact of the scheme in global climate and forecasting models.

Further work will concentrate on improving such aspects as the diagnosis and treatment of decoupled cloud layers and a more direct coupling with the mass-flux scheme used for cumulus convection.

Acknowledgments. The authors would like to thank Alan Grant for his insight into the modeling of cumulus-capped boundary layers.

APPENDIX

Definitions of the Velocity Scales

Lock (1998) derived a parameterization of the entrainment rate in convective boundary layers that was based on three velocity scales, each representative of a turbulence-generating process (V_{surf} for surface heating, V_{rad} for cloud-top radiative cooling, and V_{br} for buoyancy reversal). These were identified from large eddy simulations in which each process was acting in isolation. The velocity scales can be written

$$V_{\text{surf}}^3 = z_{\text{ml}}[(2 - \zeta)\zeta\overline{w'b'}_S + (1 - \zeta)^2[\overline{w'b'}_S]_{\text{sat}}], \quad \text{(A1)}$$

$$V_{\text{rad}}^3 = gz_{\text{ml}}\Delta_F[\beta_T\zeta^2 + \tilde{\beta}_T(1 - \zeta^2)], \quad \text{and} \quad \text{(A2)}$$

$$V_{\text{br}}^3 = A_{\text{br}}\chi_s^2 \max[0, -\delta b]\Delta b^{1/2}z_c^{3/2}C_{\text{fac}}, \quad \text{(A3)}$$

where V_{surf} and V_{rad} were evaluated, following Stage and Businger (1981), by integrating the theoretical contribution of each process to the buoyancy flux over the mixed layer. Thus, $[\overline{w'b'}_S]_{\text{sat}} = g(\tilde{\beta}_T\overline{w'\theta_l'}_S + \tilde{\beta}_q\overline{w'q_t'}_S)$, where the subscript S indicates the surface flux; $\zeta = (z_{\text{ml}} - z_c)/z_{\text{ml}}$, where z_{ml} is the mixed-layer depth and z_c is the cloud depth; Δ_F is the divergence of the net radiative flux, F (in K m s^{-1}), associated with cloud top. In the presence of significant buoyancy reversal [indicated by the Siems et al. (1990) parameter, $D = \chi_s\delta b/\Delta b \gtrsim 0.05$], Lock found that a feedback between radiative and evaporative generation of turbulence could accurately be accounted for by setting $\zeta = 1$ in (A2) and $\alpha_t = 1$ in (1).

The formula for V_{br} was derived using dimensional arguments and comparison with LES data: $\chi_s = -q_{l_{\max}}[1 + (L/c_p)\gamma_s]/(\Delta q_t - \gamma_s\Delta\theta_l)$, where $q_{l_{\max}}$ is the cloud-top liquid water mixing ratio, $\gamma_s = \partial q_s/\partial T$, L is the latent heat of vaporization of water, c_p the specific heat at constant pressure, and T is the temperature; $\delta b = g(\tilde{\beta}_T\Delta\theta_l + \tilde{\beta}_q\Delta q_T)$ and the buoyancy jump across the inversion is $\Delta b = g\{\beta_T\Delta\theta_l + \beta_q\Delta q_T + [L/c_p - (1 + \beta_q)]\Delta q_l\}$. The empirical constant $A_{\text{br}} = 0.056$.

The required jumps across cloud top are taken simply as the grid-level differences except for Δq_l and $q_{l_{\max}}$, for which in-cloud values extrapolated to grid-layer boundaries using the adiabatic lapse rate are used. The buoyancy parameters are given by $\beta_T = 1/T$, $1 + \beta_q$ ($\approx$1.608) is the ratio of the molecular weight of dry air to that of water vapor, $\tilde{\beta}_T = \beta_T - \gamma_s\beta_c$, $\tilde{\beta}_q = \beta_q + \beta_c$, and $\beta_c = [(L/c_p)\beta_T - (1 + \beta_q)]/[1 + (L/c_p)\gamma_s]$.

Note that Lock only derived his parameterization for near unbroken cloud sheets. The only explicit account of variable cloud fraction (C_F) is in (A3) for which it is assumed that buoyancy reversal can only occur for cloudy air underlying cloud-free air (assuming maximum overlap). Thus, the cloud fraction factor, $C_{\text{fac}} =$

$\max(0.0, -\Delta C_F)$. A more complete decomposition is not possible given a cloud scheme in the model (Smith 1990), which does not allow discrete identification of in-cloud and out-of-cloud profiles. The cloud fraction dependence of the radiative generation of turbulence is implicitly treated in (A2) simply by assuming the grid-box mean radiative flux divergence, Δ_F, occurs solely in the cloudy air.

REFERENCES

Albrecht, B. A., D. A. Randall, and S. Nicholls, 1988: Observations of marine stratocumulus during FIRE. *Bull. Amer. Meteor. Soc.*, **69,** 618–626.

Ayotte, K. W., and Coauthors, 1996: An evaluation of neutral and convective planetary boundary-layer parameterizations relative to large eddy simulations. *Bound.-Layer Meteor.*, **79,** 131–175.

Beljaars, A. C. M., 1991: Numerical schemes for parametrizations. *Proc. Seminar on Numerical Methods in Atmospheric Models,* Vol. II, Reading, United Kingdom, ECMWF, 1–42.

——, and A. K. Betts, 1992: Validation of the boundary layer representation in the ECMWF model. Proc. *Seminar on Validation of Models over Europe,* Vol. II, Reading, United Kingdom, ECMWF, 159–195.

Betts, A. K., 1986: A new convective adjustment scheme. Part I: Observational and theoretical basis. *Quart. J. Roy. Meteor. Soc.*, **112,** 677–691.

Bretherton, C. S., S. K. Krueger, M. C. Wyant, P. Bechtold, E. van Meijgaard, B. Stevens, and J. Teixeira, 1999: A GCSS boundary-layer cloud model intercomparison study of the first ASTEX Lagrangian experiment. *Bound.-Layer Meteor.*, **93,** 341–380.

Brown, A. R., 1996: Evaluation of parameterization schemes for the convective boundary layer using large-eddy simulation results. *Bound.-Layer Meteor.*, **81,** 167–200.

——, 1999: The sensitivity of large-eddy simulations of shallow cumulus convection to resolution and subgrid model. *Quart. J. Roy. Meteor. Soc.*, **125,** 469–482.

Cuijpers, J. W. M., and A. A. M. Holtslag, 1998: Impact of skewness and nonlocal effects on scalar and buoyancy fluxes in convective boundary layers. *J. Atmos. Sci.*, **55,** 151–162.

de Roode, S., and P. G. Duynkerke, 1997: Observed Lagrangian transition of stratocumulus into cumulus during ASTEX: Mean state and turbulence structure. *J. Atmos. Sci.*, **54,** 2157–2173.

Driedonks, A. G. M., 1982: Models and observations of the growth of the atmospheric boundary layer. *Bound.-Layer Meteor.*, **23,** 283–306.

Edwards, J., and A. Slingo, 1996: Studies with a flexible new radiation code. I: Choosing a configuration for a large-scale model. *Quart. J. Roy. Meteor. Soc.*, **122,** 689–720.

Gregory, D., and P. R. Rowntree, 1990: A mass flux scheme with representation of cloud ensemble characteristics and stability-dependent closure. *Mon. Wea. Rev.*, **118,** 1483–1506.

Hignett, P., 1991: Observations of diurnal variation in a cloud-capped marine boundary layer. *J. Atmos. Sci.*, **48,** 1474–1482.

Holtslag, A. A. M., and B. A. Boville, 1993: Local versus nonlocal boundary-layer diffusion in a global climate model. *J. Climate*, **6,** 1825–1842.

Lock, A. P., 1998: The parametrization of entrainment in cloudy boundary layers. *Quart. J. Roy. Meteor. Soc.*, **124,** 2729–2753.

——, 1999: A parametrization of turbulent mixing in convective cloud-capped boundary layers derived from large-eddy simulations. Preprints, *13th Symp. on Boundary Layers and Turbulence,* Dallas, TX, Amer. Meteor. Soc., 589–592.

Louis, J.-F., 1979: A parametric model of vertical eddy fluxes in the atmosphere. *Bound.-Layer Meteor.*, **17,** 187–202.

Mahrt, L., 1976: Mixed layer moisture structure. *Mon. Wea. Rev.*, **104,** 1403–1407.

Martin, G. M., D. W. Johnson, D. P. Rogers, P. R. Jonas, P. Minnis, and D. A. Hegg, 1995: Observations of the interaction between cumulus and stratocumulus in the marine boundary layer during ASTEX. *J. Atmos. Sci.*, **52,** 2902–2922.

——, M. R. Bush, A. R. Brown, A. P. Lock, and R. N. B. Smith, 2000: A new boundary layer mixing scheme. Part II: Tests in climate and mesoscale models. *Mon. Wea. Rev.*, 3200–3217.

Moeng, C.-H., P. P. Sullivan, and B. Stevens, 1999: Including radiative effects in an entrainment-rate formula for buoyancy driven PBLs. *J. Atmos. Sci.*, **56,** 1031–1049.

Senior, C. A., and J. F. B. Mitchell, 1993: Carbon dioxide and climate: Impact of cloud parameterization. *J. Climate,* **6,** 393–418.

Siebesma, A. P., and J. W. M. Cuijpers, 1995: Evaluation of parametric assumptions for shallow cumulus convection. *J. Atmos. Sci.*, **52,** 650–666.

Siems, S. T., C. S. Bretherton, M. B. Baker, S. Shy, and R. E. Breidenthal, 1990: Buoyancy reversal and cloud-top entrainment instability. *Quart. J. Roy. Meteor. Soc.*, **116,** 705–739.

Smith, R. N. B., 1990: A scheme for predicting layer clouds and their water content in a general circulation model. *Quart. J. Roy. Meteor. Soc.*, **116,** 435–460.

Stage, S. A., and J. A. Businger, 1981: A model for entrainment into a cloud-topped marine boundary layer. Part I: Model description and application to a cold-air outbreak episode. *J. Atmos. Sci.*, **38,** 2213–2229.

Troen, I. W., and L. Mahrt, 1986: A simple model of the atmospheric boundary layer; sensitivity to surface evaporation. *Bound.-Layer Meteor.*, **37,** 129–148.

Turton, J. D., and S. Nicholls, 1987: A study of the diurnal variation of stratocumulus using a multiple mixed layer model. *Quart. J. Roy. Meteor. Soc.*, **113,** 969–1009.

van Meijgaard, E., and A. P. van Ulden, 1998: A first-order mixing-condensation scheme for nocturnal stratocumulus. *Atmos. Res.*, **45,** 253–273.

Vogelezang, D. H. P., and A. A. M. Holtslag, 1996: Evaluation and model impacts of alternative boundary-layer height formulations. *Bound.-Layer Meteor.*, **81,** 245–269.

Zilitinkevich, S. S., 1975: Comments on ''A model for the dynamics of the inversion above a convective boundary layer.'' *J. Atmos. Sci.*, **32,** 991–992.